






# Ideal-lens cloaks and new cloaking strategies

JAKUB BĚLÍN,<sup>1,\*</sup>  TOMÁŠ TYC,<sup>2</sup> MATEUSZ GRUNWALD,<sup>1</sup> STEPHEN OXBURGH,<sup>1</sup> EUAN N. COWIE,<sup>1</sup>  CHRIS D. WHITE,<sup>3</sup> AND JOHANNES COURTIAL<sup>1</sup> 

<sup>1</sup>*School of Physics & Astronomy, University of Glasgow, Glasgow G12 8QQ, UK*

<sup>2</sup>*Institute of Theoretical Physics and Astrophysics, Masaryk University, Kotlářská 2, 61137 Brno, Czech Republic*

<sup>3</sup>*Centre for Research in String Theory, Queen Mary University of London, 327 Mile End Road, London E1 4NS, UK*

\*[j.belin.1@research.gla.ac.uk](mailto:j.belin.1@research.gla.ac.uk)

**Abstract:** Previously [Courtial *et al.*, *Opt. Express* **26**, 17872 (2018)] we presented the theory of transformation optics (TO) with ideal lenses and demonstrated an example, an omnidirectional lens. Here we interpret this omnidirectional lens in two different parameter regimes as ideal-lens cloaks that employ different cloaking strategies: a standard “shrink cloak” in which objects appear smaller (ideally zero) and a novel “abyss cloak” in which interior physical-space positions are mapped to the exterior and thus are visible only from certain directions. We proceed to combine two nested abyss cloaks into another novel, omnidirectional, “bi-abyss cloak.” Our work significantly extends the arsenal of cloaking strategies.

Published by The Optical Society under the terms of the [Creative Commons Attribution 4.0 License](https://creativecommons.org/licenses/by/4.0/). Further distribution of this work must maintain attribution to the author(s) and the published article's title, journal citation, and DOI.

## 1. Introduction

Transformation optics (TO) [1,2] is the science of using a material structure to distort light-ray trajectories within the structure such that the apparent shape and/or size of any object inside it is changed. The actual structure is said to be in physical space, whereas the apparent structure as seen from the outside is said to be in virtual (or electromagnetic) space; the ‘transformation’ refers to the mapping between positions in physical space and virtual space. The ideas of TO have been applied to other branches of physics, resulting, for example, in transformation thermodynamics [3,4], acoustic cloaking [5], elastic cloaking [6], and seismic cloaking [7].

Probably the most publicised potential application of TO is invisibility cloaking [1,2,8–12], which makes a volume inside the physical TO structure – and the structure itself – invisible from outside of the structure. This invisibility of the structure itself is important, as it is, of course, very easy to make a volume invisible, for example by enclosing it in a box, but in this case, the box, and the fact that there is a hidden volume inside it, is clearly visible. In TO invisibility cloaks, the cloak itself is, in principle, invisible.

When viewed from the outside, the invisibility cloaks proposed in Refs [1,2,9] guide light rays entering the cloak from the outside such that they never pass through a cloaked volume inside the cloak and emerge from the cloak on the same straight-line trajectory on which they entered. This implies that no light rays that originate in the cloaked volume can leave the cloak, so any objects inside the cloaked volume are invisible from the outside. As light rays that enter the cloak from the outside emerge from the cloak undistorted, the cloak is (in the absence of other effects on light rays, such as absorption or phase or polarisation changes) itself invisible. Many invisibility cloaks can be seen as structures that appear to shrink a “cloaked” interior volume to a volume of zero size; for example, the cloak proposed in [2] appears to shrink a sphere into a point. There are other types of invisibility cloak, including the carpet cloak [8,12]: like an actual

carpet draped over an object lying on the floor, it hides the object; unlike an actual carpet, which visibly forms a “bump” over the object, the carpet cloak appears to have the same shape as the floor. All of these invisibility cloaks create the illusion of empty space where there is actually an optical device and therefore can be regarded as a special case of illusion optics [13].

Practical realisations of TO invisibility cloaks require highly advanced material engineering and some designs cannot be realised at all [14]. Due to these limitations, several research groups considered “ray-optical” cloaks, which relax requirements on phase and which only work for a limited number of viewing directions, but which can be built using natural materials [15,16] or simple optical elements. The “Rochester cloak” [17], a combination of four coaxial lenses, is a striking example: when viewed from a small range of directions, there are several regions through which no light rays seen by the observer have passed, and therefore an object can be

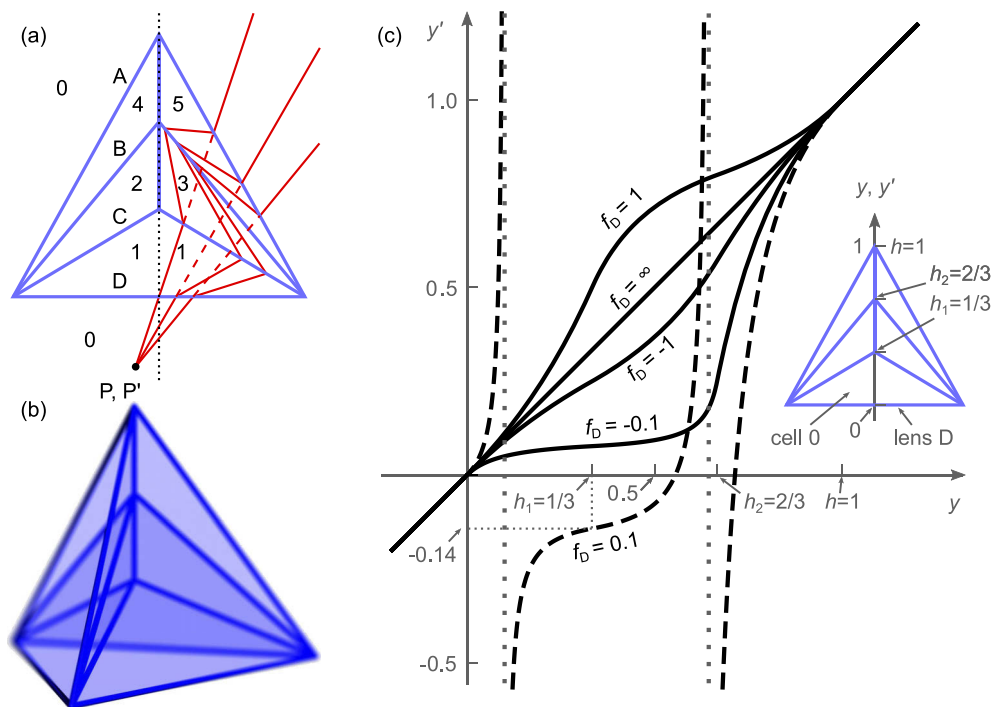


**Fig. 1.** Structure of, and imaging in, the ideal-lens structure that can be interpreted as an omnidirectional lens or as an ideal-lens cloak. The structure is shown in 2D (a) and in 3D (b); the ideal thin lenses are shown as blue lines in (a) and as blue, semi-transparent, triangles whose edges are shown as blue cylinders in (b). In (a), a few lenses are marked A to D; the optical axis of lens D is marked as a dotted black line. The lenses divide physical space inside the device into cells (polygonal in 2D, polyhedral in 3D) numbered 1, 2, 3, etc.; cell 0 is the outside of the device. A number of light-ray trajectories (solid red lines) passing through the structure, originating from a point source P outside the structure, are shown in (a). The straight-line continuations (dashed red lines) of the outside segments of those same light-ray trajectories intersect in virtual space position  $P' = P$ . The relationship between axial positions in physical and virtual space in an omnidirectional lens, plotted for a number of values of  $f_D$ , is shown in (c).  $y$  and  $y'$  are heights above lens D of a position in physical space and in virtual space, respectively. The curves were calculated for a structure whose geometry is given by the values  $h_1 = 1/3$ ,  $h_2 = 2/3$ ,  $h = 1$ . Cell 1 corresponds to the range  $0 < y < h_1$ .

hidden in these regions. As the viewing positions for which this cloak works are limited to the vicinity of the lenses' common optical axis, the "Rochester cloak" is a paraxial cloak.

Recently, we constructed a theoretical ray-optical transformation-optics (RTO) device from ideal thin lenses (Figs. 1(a) and (b)), aiming to realise key features of such a device with physical lenses later [18]. Any object placed inside the ideal-lens structure appears distorted when viewed from outside of the structure; the distortion is the same from any viewing direction; and any objects seen *through* the structure appear undistorted (see App. B). When an object is placed in certain regions, the distortion — the 3D mapping between physical (object) positions and their apparent (image) positions when viewed from the outside — is that of an ideal lens, and as the distorted object can be viewed from *any* direction, this structure is an *omnidirectional lens*.

Here we investigate this lens structure further. We discuss the mapping between physical space and virtual space and show that, in two different parameter regimes, the lens structure can be interpreted as an invisibility cloak, and for this reason the lens structure is also an *ideal-lens cloak*. Our ideal-lens cloak can act as two different types of invisibility cloak: depending on the choice of the parameters of the structure, it can either reduce the size of a volume inside it when seen from any direction ("omnidirectional shrink cloak"), in principle to zero; or it can function as a novel type of cloak we call an *abyss cloak*, which can hide objects from a range of directions ("semidirectional"). We also show how to use two nested, semidirectional, abyss cloaks to construct an omnidirectional cloak we call an "bi-abyss cloak".

The structure of this paper is as follows. We examine the mapping between physical space and virtual space in the ideal-lens cloak in section 2. In section 3., we use this mapping to construct different cloaking strategies. This is followed by a concluding discussion (Sec. 4.).

## 2. Mapping between physical and virtual space

The mapping between physical space and virtual space depends on the geometry of the lens structure and the choice of focal lengths. In general, this mapping is different for each cell: in the case of the outer cells (1, 4 and 5 in Fig. 1(a)), it is that due to the lens separating the cell from the outside; for the inner cells (2 and 3 in Fig. 1(a)), which are separated from the outside by two lenses, it is the combination of the mappings due to these two lenses. The mapping due to each individual lens is continuous (provided points at infinity in opposite directions are identified), and therefore the mapping by the structure as a whole is continuous as well.

For our purposes it is useful to calculate the virtual-space positions corresponding to physical-space positions on the optical axis of lens D in a particular example of an omnidirectional lens. As our example, we choose an omnidirectional lens in which the lower inner vertex, the upper inner vertex, and the top vertex are respectively a height  $h_1 = 1/3$ ,  $h_2 = 2/3$ , and  $h = 1$  above lens D; Fig. 1 is drawn for those ratios. Following [18], we choose the focal length of lens D and calculate the focal lengths of the other lenses. As lens D (like any lens) images positions on its optical axis to other positions on its optical axis, the corresponding virtual-space positions all lie on the optical axis of lens D again. We describe their position on this optical axis by the height above lens D:  $y$  is the height above lens D of a physical-space position,  $y'$  is that of the corresponding virtual-space position. Figure 1(c) shows the relationship between  $y$  and  $y'$ , derived in App. C, for a number of different values of the focal length of lens D,  $f_D$ . Outside of the structure, that is, in cell 0, which corresponds to heights above lens D of  $y < 0$  and  $y > h$ , virtual space and physical space coincide in all cases, so  $y' = y$ . In cell 1, that is for  $0 < y < h_1$ , the mapping is that due to lens D alone, and so

$$\frac{1}{y} - \frac{1}{y'} = \frac{1}{f_D}. \quad (1)$$

Looking out of the inner cells, cells 2 and 3, means looking through at least two skew lenses, namely B and A or C and D, resulting in a more complex mapping.

### 3. Cloaking strategies

We identify three distinct strategies — one well-known, the other two new — which can be employed to turn the omnidirectional lens into an invisibility cloak.

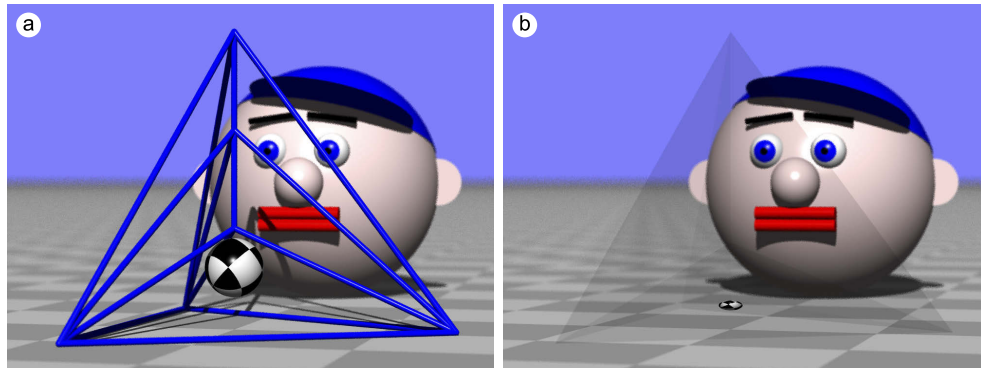
The first, well-known, cloaking strategy is based on the observation that, whenever the virtual-space image of an object inside the cloak is de-magnified, it is less visible than the object itself. In the limit of de-magnification to size zero, the virtual-space image is completely invisible, which is the “classical” cloaking strategy employed in [2]. Note, however, that in the ideal-lens cloak this limit corresponds to the case  $f_D = 0$ , which is impossible to reach even if ideal lenses existed.

In the curves shown in Fig. 1(c), de-magnification of the image corresponds to a slope of magnitude less than 1:

$$\left| \frac{dy'}{dy} \right| < 1. \quad (2)$$

Note that the fact that longitudinal magnification is the square of transverse magnification (which is a general property of imaging by a single ideal lens) then implies de-magnification also in the horizontal direction.

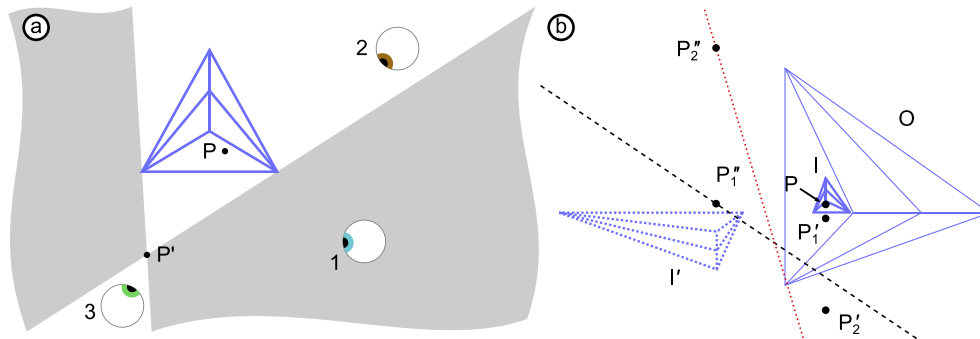
This de-magnification in all directions of the virtual-space image of an object inside the cloak is clearly demonstrated in Fig. 2. Note also that any object seen through the cloak, such as the head, floor and sky, are seen undistorted, which is the mapping required to make the cloak invisible. That the cloak is nevertheless (slightly) visible in Fig. 2(b) is due to the ideal lenses having been programmed to be slightly absorbing.



**Fig. 2.** Raytracing simulations of an ideal-lens shrink cloak. (a) Physical-space structure, where each face bounded by blue cylinders is a lens. A chequered sphere is placed inside the structure. (b) Visual appearance of the device with cylinders removed and all ideal lenses (made visible by making them slightly absorptive) in place. The appearance is now that of electromagnetic space; any object inside the structure is distorted, any object outside it is not. The chequered sphere now appears distorted, displaced, and de-magnified. Both images are the initial frames of movies, available at [19], in which the camera position is varied. Details about the raytracing simulations can be found in App. A.

The second cloaking strategy is based on the observation that physical-space positions inside the cloak can be imaged to virtual-space positions *outside* of the cloak; in the curves shown in Fig. 1(c), this is the case whenever  $0 < y < 1$  and either  $y' < 0$  or  $y' > 1$ . Figure 3(a) sketches the case when an interior point P is imaged to a virtual-space position P' below lens D, which corresponds to the case  $y' < 0$ . Figure 3(a) also indicates three viewing positions. From viewing position 1, the image at P' cannot be visible, as P' is simply a position in empty space seen along a line of sight that does not intersect any of the lenses that form the cloak. The image at P'

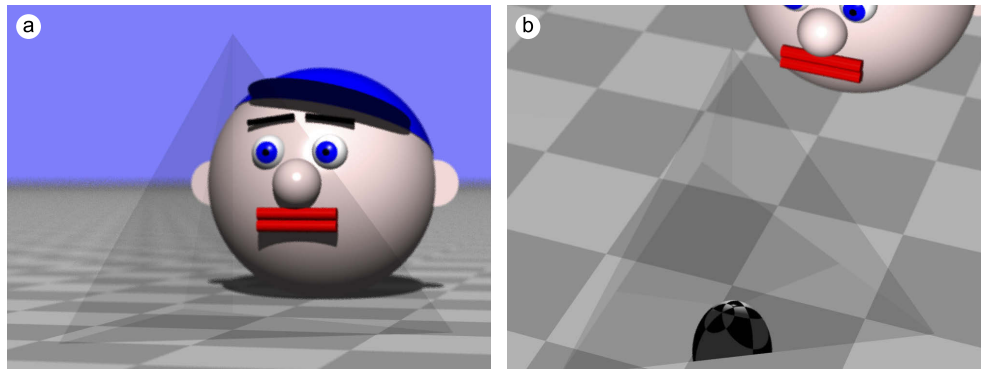
can only be visible along lines of sight that intersect both  $P'$  and the cloak. In other words, the image can be visible only in line with the cloak, that is, either behind or in front of it, which is respectively the case for viewing positions 2 and 3. The shaded area shown in Fig. 3(a) is the totality of all viewing positions from which  $P'$  cannot be visible; this area has been constructed such that no line of sight that intersects both  $P'$  and the cloak passes through it.



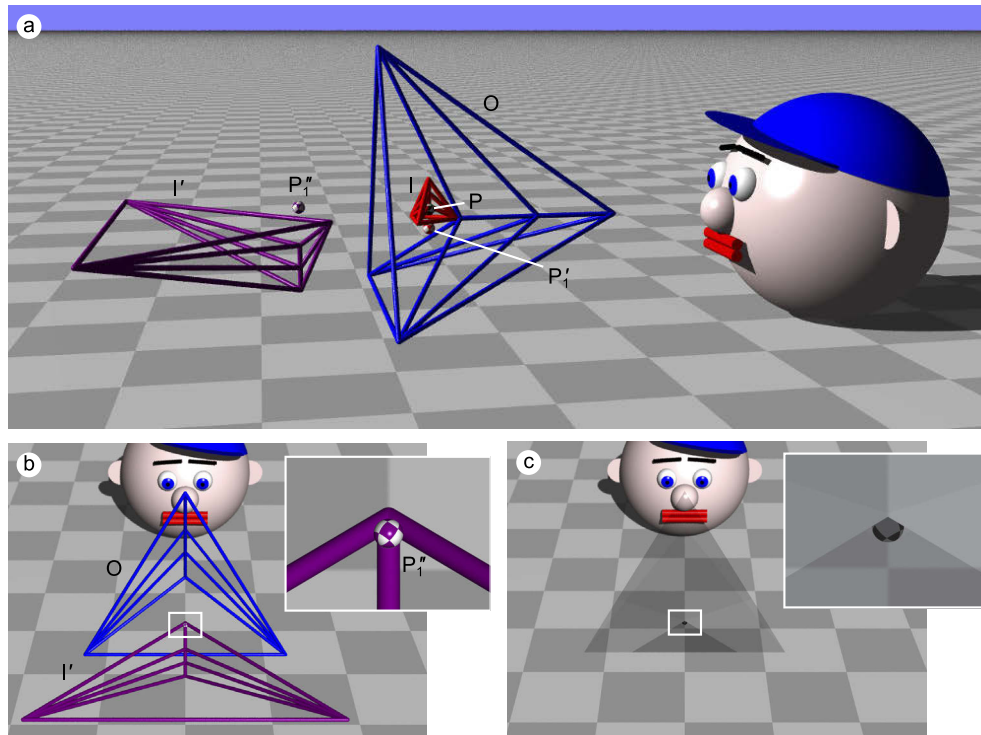
**Fig. 3.** Principle of the abyss cloak (a) and of the bi-abyss cloak (b). (a) The abyss cloak images a physical-space position  $P$  inside the cloak to a virtual-space position  $P'$  outside the cloak. The image  $P'$  can be visible only when  $P'$  is seen in the same direction as the cloak. The shaded area in (a) indicates the positions from which this is not the case, that is the positions from which  $P'$  cannot be visible. Eyeballs indicate three example viewing positions, labelled 1 to 3;  $P'$  can be visible only from positions 2 and 3, but not from position 1. (b) In the bi-abyss cloak, an inner abyss cloak ( $I$ ; thick solid lines) is nested inside an outer abyss cloak ( $O$ ; thin solid lines). The outer cloak creates a virtual-space image of the inner cloak ( $I'$ ; dotted lines). According to a choice of parameters of cloaks  $O$  and  $I$ , two different cases may happen: in the first case, a point  $P$  inside the inner cloak,  $I$ , is imaged by  $I$  to  $P'_1$ , which is re-imaged by the outer cloak,  $O$ , to  $P''_1$ , such that there exist lines of sight (such as the dashed line shown) that simultaneously intersect  $P''_1$ ,  $I'$  and  $O$ .  $P''_1$  is visible along such lines of sight. In the second case, the image  $P''$  of  $P$  due to both cloaks,  $I$  and  $O$ , is located such that no line of sight through  $P''_2$ ,  $I'$  and  $O$  exists. The dotted line through  $P''_2$ , for example, passes through  $O$ , but not  $I'$ . The point  $P$  is therefore invisible from the outside.

Figure 4 demonstrates this idea. It shows raytracing simulations of an ideal-lens cloak with the physical-space geometry shown in Fig. 2(a) and with the focal lengths of the ideal lenses chosen such that the chequered sphere inside the cloak (also shown in Fig. 2(a)) is imaged to a virtual-space position below the cloak. In Fig. 4(a) the camera is positioned such that no part of the image of the sphere lines up with the cloak, and so it is invisible. When the camera is moved such that part of the image of the sphere is seen (b) in line with the cloak (specifically, the image of the sphere is located behind the cloak), those parts of the image of the sphere become visible. The sphere appears to be located inside a bottomless cavity — an abyss — opening at the cloak. For this reason, we call this configuration an *abyss cloak*.

The third cloaking strategy hides an object inside two nested abyss cloaks. The inner abyss cloak,  $I$ , images a position  $P$  inside  $I$  to a position  $P'$  external to  $I$ ; the outer abyss cloak,  $O$ , creates images  $P''$  and  $I'$  of  $P'$  and  $I$ , respectively, both external to  $O$ . As discussed above,  $P'$  can be visible only along lines of sight where it is in line with  $I$ . Now  $O$  appears as the opening into an abyss that includes  $I'$ , which in turn appears as the opening into another abyss that includes  $P''$ , and so  $P''$  can be visible only “through both abyss openings”, that is, along lines of sight where  $P''$  lines up with both  $I'$  and  $O$ . Figure 3(b) illustrates that there are configurations in which there is not a single line of sight along which  $P''$  lines up with both  $I'$  and  $O$ . It is drawn for two different values of the focal length of the base lens of the inner cloak; in the first case, the



**Fig. 4.** Raytracing simulations of an ideal-lens abyss cloak. The physical-space geometry is the same as that shown in Fig. 2(a), including the chequered sphere inside the cloak. (a) If the camera is positioned outside the region from which any part of the image of the sphere is aligned with the cloak, the sphere is hidden. (b) If the camera is situated such that part of the image of the sphere is aligned with the cloak, that part of the image is visible. The images are part of a movie available at [19]. Details of the simulations can be found in App. A.



**Fig. 5.** Raytracing simulations of an ideal-lens bi-abyss cloak. (a) Geometry of the outer abyss cloak, O (blue structure), the inner abyss cloak, I (red structure), the image  $I'$  of I due to O (purple structure), and a position P inside I and its images  $P_1'$  and  $P_1''$  due to I and the combination of I and O, respectively (chequered spheres). (b) Like (a), but seen along a line of sight for which  $P_1''$  is aligned with  $I'$  and O. (c) Like (b), but with the blue and purple structures that indicated the geometry of O and  $I'$  in (a) and (b) removed and all ideal lenses in place. The images shown in (b) and (c) are part of movies available at [19].

image of  $P$  due to  $I$  is  $P'_1$  and that due to the combination of  $I$  and  $O$  is  $P''_1$ , in the second case the images are  $P'_2$  and  $P''_2$ . The first case is chosen such that there are lines of sight (such as the one shown) where  $P'_1$  lines up with  $I'$  and  $O$ ;  $P'_1$  can therefore be visible along such lines of sight, and raytracing simulations (Figs. 5(a)-(c)) confirm this. The second case is chosen such that there are *no* lines of sight along which  $P'_2$  lines up with  $I'$  and  $O$ ;  $P'_2$  is thus invisible from any position outside  $O$ , along *any* line of sight. Numerous raytracing simulations in which the image  $P'_2$  is not visible confirmed this, but are not shown for lack of anything to see. The resulting structure is therefore an omnidirectional cloak; we call it *bi-abbyss cloak*.

#### 4. Conclusions

We have presented two new cloaking strategies based on the previously proposed omnidirectional lens. The first strategy results in an abyss cloak that is able to hide an object completely from being observed from certain spatial regions. The second strategy uses a suitable combination of two nested abyss cloaks to achieve complete, omnidirectional, invisibility. Remarkably, both cloaks are composed solely from ideal lenses.

The new cloaking strategies were developed for structures comprising ideal lenses. These are theoretical idealisations that cannot exist in reality as this is forbidden by Maxwell's theorem [20], but there might be a number of ways around this. Firstly, it might be possible to realise these cloaking strategies experimentally with real lenses or Fresnel lenses such that they work either "paraxially" (for viewing directions close to a central "axial" direction) or for one or two viewing positions [18]. Either way, the optical path length through the device would depend on which cells the ray passes through, and in any case would be longer than that through air, in the absence of the device. The second possibility would be the use of metalenses — metasurfaces that aim to mimic ideal lenses as closely as possible — which are developing rapidly [21–23]. Thirdly, it might be possible to realise the new cloaking strategies using metamaterial structures, which would be closely related to, but different from, the "anticloak" [24], in that they would image interior points to the outside. We are currently working on the design and initial wave-optical analysis of precisely such structures [25].

##### A. Raytracing simulations

The simulations were performed using an extended version of our custom, open-source [26], raytracer Dr TIM [27]. Dr TIM is written in Java for ease of portability between platforms.

As is standard in rendering raytracing, Dr TIM traces rays backwards, starting from the camera, via scene objects, to a light source. Dr TIM has the ability to simulate idealised components such as ideal thin lenses, which simply change the direction of transmitted light rays.

For the simulations in this paper, Dr TIM was compiled into two Java Applications, `LensCloakVisualiser` (which was used to calculate the images shown in Figs. 2 and 4) and `NestedAbyssCloakExplorer` (with which the images shown in Fig. 5 were calculated), which are available at [19]. Text files that list the values of the parameters of the different simulations, one text file per simulation, are also available at [19].

##### B. Imaging in ray-optical transformation-optics devices and the omnidirectional lens

We define a ray-optical transformation-optics (RTO) device by the existence of a unique mapping from physical space to virtual space. For the lens structure shown in Fig. 1 to be an RTO device, any position in any of the cells of the lens structure has to be mapped to the same position in cell 0 *irrespective of which lenses the light rays from that position pass through on their way to cell 0*. In other words, when looking from the outside (cell 0) at a point object inside one of the

cells inside the lens structure, the image of the point object is seen at the same position from any direction.

If we want to design a lens structure that is an RTO device, we need to ensure that images of any point in physical space due to different subsets of lenses included in the structure coincide. This demand leads to the *loop-imaging condition* [18], which requires that the combination of all optical elements encountered along any closed loop must image every position back to itself.

There are, of course, infinitely many different closed loops that could be considered. Therefore a different condition has been formulated, the *edge-imaging condition* for a common edge shared by a number of lenses, which is satisfied if and only if successive imaging by all lenses sharing the edge yields the identity mapping [18]. Whether or not a lens structure is an RTO device can then be determined using the *edge-imaging theorem* [18], which states that a lens structure is an RTO device if and only if every edge in the device satisfies the edge-imaging condition.

From the edge-imaging condition, we derived the following necessary conditions on two, three and four ideal thin lenses sharing a common edge [28]:

- If two lenses share a common edge, their principal points and principal planes must coincide.
- If three lenses share a common edge, their principal points must coincide.
- If four lenses share a common edge, their principal points must lie on a straight line.

Additional necessary conditions on the focal lengths of the lenses can be derived from the edge-imaging condition [18].

### C. Derivation of the equations describing the mapping on the optical axis of lens D

We start from the equations for the focal lengths of the lenses in an omnidirectional lens, [18]

$$f_A = -\frac{(h_2 - h)(f_D(h_1 - h) + h_1 h)R}{h_1 h_2 \sqrt{4h^2 + R^2}}, \quad (3)$$

$$f_B = \frac{f_D(h_1 - h_2)(h_2 - h)R}{h_1 h \sqrt{4h_2^2 + R^2}}, \quad (4)$$

$$f_C = -\frac{(h_1 - h_2)(f_D(h_1 - h) + h_1 h)R}{h_2 h \sqrt{4h_1^2 + R^2}}, \quad (5)$$

where  $f_D$  is the focal length of the base lens (lens D),  $h$ ,  $h_2$  and  $h_1$  are the heights of the principal points of lenses A, B and C above lens D, and  $R$  is the circumradius of the (triangular) base lens. In order to find the virtual-space positions of objects lying on the optical axes (the line passing through all the principal points of lenses A, B, C and D), it turns out to be convenient to calculate the projected focal lengths  $g_i = f_i / \cos \varphi_i$ , where  $\varphi_i$  is the angle between the normal of lens  $i$  ( $i = A, B, C, D$ ) and the optical axis [29]. One can deduce easily that  $\cos \varphi_A = R / \sqrt{4h^2 + R^2}$ ,



$\cos \varphi_B = R/\sqrt{4h_2^2 + R^2}$  and  $\cos \varphi_C = R/\sqrt{4h_1^2 + R^2}$  and thus

$$g_A = -\frac{(h_2 - h)(f_D(h_1 - h) + h_1h)}{h_1h_2}, \quad (6)$$

$$g_B = \frac{f_D(h_1 - h_2)(h_2 - h)}{h_1h}, \quad (7)$$

$$g_C = -\frac{(h_1 - h_2)(f_D(h_1 - h) + h_1h)}{h_2h}. \quad (8)$$

These formulas are significantly simplified for a case  $h_1 = h/3$  and  $h_2 = 2h/3$ , which yields the formulas

$$g_A = \frac{h}{2} - f_D, \quad (9)$$

$$g_B = \frac{f_D}{3}, \quad (10)$$

$$g_C = \frac{g_A}{3} = \frac{h}{6} - \frac{f_D}{3}. \quad (11)$$

Now we can find the virtual-space positions of object lying on the optical axis. An object with a  $y$ -coordinate  $q_1 \in (2h/3, h)$  is imaged to the outside due to lens A and the virtual space-position  $y'_1$  satisfies the imaging equation

$$y'_1 = h + \frac{g_A(y_1 - h)}{g_A + y_1 - h} = h + \frac{(h/2 - f_D)(y_1 - h)}{h/2 - f_D + y_1 - h}. \quad (12)$$

If the object lies on the optical axis at in the range  $y_2 \in (h/3, 2h/3)$ , the final image (or virtual-space position) is then due to the combination of lenses B and A. Lens B provides a  $y$  coordinate of the image

$$y''_2 = \frac{2h}{3} + \frac{g_B(y_2 - 2h/3)}{g_B + y_2 - 2h/3} = \frac{2h}{3} + \frac{f_D(y_2 - 2h/3)}{f_D + 3y_2 - 2h}; \quad (13)$$

lens A then provides the  $y$  coordinate of the final image,

$$y'_2 = h + \frac{g_A(y''_2 - h)}{g_A + y''_2 - h} = h + \frac{(h/2 - f_D)(y''_2 - h)}{h/2 - f_D + y''_2 - h} = -\frac{f_D [2h^2 - (6f_D + 3h)y_2]}{6f_D^2 - 9f_Dh + 2h^2 + 3(4f_D - h)y_2}. \quad (14)$$

Finally, the object with a coordinate  $y_3 \in (0, h/3)$  is imaged outside due to a combination of lenses C, B and A. However, the edge-imaging condition can be applied and it is possible to show that the image  $y'_3$  due to that combination is the same as the one due to a single lens with focal length  $-f_D$ , namely

$$y'_3 = \frac{-f_D y_3}{-f_D + y_3}. \quad (15)$$

## Funding

Engineering and Physical Sciences Research Council (EP/M/010724/1, EP/N/509668/1).

## Disclosures

The authors declare no conflicts of interest.

## References

1. U. Leonhardt, "Optical conformal mapping," *Science* **312**(5781), 1777–1780 (2006).
2. J. B. Pendry, D. Schurig, and D. R. Smith, "Controlling electromagnetic fields," *Science* **312**(5781), 1780–1782 (2006).
3. R. Schittny, M. Kadic, S. Guenneau, and M. Wegener, "Experiments on transformation thermodynamics: Molding the flow of heat," *Phys. Rev. Lett.* **110**(19), 195901 (2013).
4. R. Hu, X. Wei, J. Hu, and X. Luo, "Local heating realization by reverse thermal cloak," *Sci. Rep.* **4**(1), 3600 (2015).
5. B.-I. Popa, L. Zigoneanu, and S. A. Cummer, "Experimental acoustic ground cloak in air," *Phys. Rev. Lett.* **106**(25), 253901 (2011).
6. N. Stenger, M. Wilhelm, and M. Wegener, "Experiments on elastic cloaking in thin plates," *Phys. Rev. Lett.* **108**(1), 014301 (2012).
7. S. Brûlé, E. H. Javelaud, S. Enoch, and S. Guenneau, "Experiments on seismic metamaterials: Molding surface waves," *Phys. Rev. Lett.* **112**(13), 133901 (2014).
8. J. Li and J. B. Pendry, "Hiding under the carpet: A new strategy for cloaking," *Phys. Rev. Lett.* **101**(20), 203901 (2008).
9. U. Leonhardt and T. Tyc, "Broadband Invisibility by Non-Euclidean Cloaking," *Science* **323**(5910), 110–112 (2009).
10. B. Zhang, Y. Luo, X. Liu, and G. Barbastathis, "Macroscopic invisibility cloak for visible light," *Phys. Rev. Lett.* **106**(3), 033901 (2011).
11. Y. Lai, H. Chen, Z.-Q. Zhang, and C. T. Chan, "Complementary media invisibility cloak that cloaks objects at a distance outside the cloaking shell," *Phys. Rev. Lett.* **102**(9), 093901 (2009).
12. X. Ni, Z. J. Wong, M. Mrejen, Y. Wang, and X. Zhang, "An ultrathin invisibility skin cloak for visible light," *Science* **349**(6254), 1310–1314 (2015).
13. Y. Lai, J. Ng, H. Chen, D. Han, J. Xiao, Z.-Q. Zhang, and C. T. Chan, "Illusion optics: The optical transformation of an object into another object," *Phys. Rev. Lett.* **102**(25), 253902 (2009).
14. F. Monticone and A. Alù, "Invisibility exposed: physical bounds on passive cloaking," *Optica* **3**(7), 718–724 (2016).
15. H. Chen and B. Zheng, "Broadband polygonal invisibility cloak for visible light," *Sci. Rep.* **2**(1), 255 (2012).
16. H. Chen, B. Zheng, L. Shen, H. Wang, X. Zhang, N. Zheludev, and B. Zhang, "Ray-optics cloaking devices for large objects in incoherent natural light," *Nat. Commun.* **4**(1), 2652 (2013).
17. J. S. Choi and J. C. Howell, "Paraxial ray optics cloaking," *Opt. Express* **22**(24), 29465–29478 (2014).
18. J. Courtial, T. Tyc, J. Běln, S. Oxburgh, G. Ferenczi, E. N. Cowie, and C. D. White, "Ray-optical transformation optics with ideal thin lenses makes omnidirectional lenses," *Opt. Express* **26**(14), 17872–17888 (2018).
19. J. Courtial, J. Běln, T. Tyc, C. D. White, S. Oxburgh, E. N. Cowie, and M. Grunwald, "Ideal-lens cloak movies, data files and software," Figshare, <http://doi.org/10.6084/m9.figshare.9976499.v3> (2019).
20. M. Born and E. Wolf, *Principles of Optics* (Pergamon Press, Oxford, 1980), chap. 4.2.1.
21. M. Khorasaninejad, W. T. Chen, R. C. Devlin, J. Oh, A. Y. Zhu, and F. Capasso, "Metalenses at visible wavelengths: Diffraction-limited focusing and subwavelength resolution imaging," *Science* **352**(6290), 1190–1194 (2016).
22. W. T. Chen, A. Y. Zhu, V. Sanjeev, M. Khorasaninejad, Z. Shi, E. Lee, and F. Capasso, "A broadband achromatic metalens for focusing and imaging in the visible," *Nat. Nanotechnol.* **13**(3), 220–226 (2018).
23. S. Shrestha, A. C. Overvig, M. Lu, A. Stein, and N. Yu, "Broadband achromatic dielectric metalenses," *Light: Sci. Appl.* **7**(1), 85 (2018).
24. H. Chen, X. Luo, H. Ma, and C. Chan, "The anti-cloak," *Opt. Express* **16**(19), 14603–14608 (2008).
25. J. Courtial, J. Běln, and T. Tyc, "Shifty invisibility cloaks," in preparation (2019).
26. "Dr TIM, a highly scientific raytracer," <https://github.com/jkcuk/Dr-TIM>.
27. S. Oxburgh, T. Tyc, and J. Courtial, "Dr TIM: Ray-tracer TIM, with additional specialist capabilities," *Comput. Phys. Commun.* **185**(3), 1027–1037 (2014).
28. T. Tyc, J. Běln, S. Oxburgh, C. D. White, E. N. Cowie, and J. Courtial, "Glens combinations that satisfy the edge-imaging condition of transformation optics," *J. Opt. Soc. Am. A* (in press) (2019).
29. J. Běln and J. Courtial, "Imaging with two skew ideal lenses," *J. Opt. Soc. Am. A* **36**(1), 132–141 (2019).